Hindawi
International Journal of RF and Microwave Computer-Aided Engineering
Volume 2023, Article ID 4500294, 15 pages
https://doi.org/10.1155/2023/4500294

Research Article

Wide E-Plane Beamwidth Microstrip Patch Antenna Using H-Shaped Gap-Coupling with Three Parasitic Patches for the K-Band

Jeong-Hun Park and Moon-Que Lee

School of Electrical and Computer Engineering, University of Seoul, Seoul, Republic of Korea

Correspondence should be addressed to Moon-Que Lee; mqlee@uos.ac.kr

Received 15 November 2022; Revised 30 May 2023; Accepted 31 May 2023; Published 19 June 2023

Academic Editor: N. Nasimuddin

This article presents a new wide E-plane beamwidth rectangular microstrip patch antenna adopting H-shaped gap-coupling with three parasitic patches for the K-band vehicle parking monitoring system, while keeping single substrate. Both side and upper parasitic elements serve as λ and $\lambda/2$ resonators and are excited primarily by magnetic and electric couplings, respectively. The synthesis of radiation patterns from main and auxiliary elements results in the E-plane wide-beamwidth property. The proposed gap-coupling antenna provided the peak gain of 4.82 dBi, E-plane half-power beamwidth (HPBW) of 143.4°, and co-to-cross-pol ratios of 22.7 and 20.2 dB within the HPBW for the E- and H-planes, respectively. The presented geometry showed excellent figure of merits compared with others for the K-band.

1. Introduction

A wide beamwidth in antennas is beneficial for maximizing the area of coverage in a point-to-multipoint wireless communication system [1], a wide scanning range of phased array systems [2], global positioning satellite (GPS) applications [3], and smart multistandard wireless devices like communication-enabled smart vehicles [4]. For the vehicle parking monitoring system using a radar sensor with wide-angle object detection, the antenna should satisfy the requirement of wide beamwidth. In addition to that, the horizontal polarization is preferred for automotive radar target detection since the horizontally polarized backscattering coefficients are smaller than the vertically polarized backscattering coefficients for dry and wet asphalts at large incidence angles of 25° to 80° at 24 GHz [5, 6].

Various approaches have been studied to achieve the wide-beamwidth characteristics. The first technique adds an extra resonator [7] or parasitic elements [1, 6, 8–10]. The second introduces a composite dielectric substrate [11], high-permittivity substrate [12], or extended dielectric substrate [13]. The third uses an extra reflector or ground plane [14–17], while the fourth extends the substrate dimension [18, 19]. The fifth uses a Huygens source antenna based on magnetic and electric near-field resonant parasitic (NFRP) [20–22]. Finally, the sixth uses a magnetoelectric dipole antenna—where an electric monopole or dipole antenna and magnetic dipole antenna are simultaneously excited [23–27]—or a planar magnetic dipole antenna—where the magnetic dipole antenna is solely excited [2, 28–33]. Besides these approaches, a triangular substrate-integrated waveguide (SIW) antenna [34], coupled-fed printed dipole antenna [35], pyramidal configuration [36], coupled-mode patch [37], and grid array antenna [38] have been introduced. Especially, for the K-band operation, antenna structures using parasitic loop and mushroom-like elements [6], magnetic dipole [33], coupled-mode patch [37], and grid array [38] provide the wide-beamwidth property with the feeds of a through

Table 1: Advantages and disadvantages of wide-beamwidth antenna techniques.

	Size (compared with a general patch ant.)	Planar single-substrate structure	Low profile	Easy integration with other components
Hybrid zeroth-order resonance	Same	Yes	Yes	No
Parasitic element	Same	No	Yes or no	Yes or no
	Larger	Yes	Yes	Yes
Composite dielectric substrate, high-permittivity substrate, or extended dielectric substrate	Same or smaller	No	No	No
Extra reflector or ground plane	Same	No	No	No
Huygens source antenna based on magnetic and electric near-field resonant parasitic	—	No	No	No
Magnetoelectric dipole antenna	—	No	No	No
Planar magnetic dipole antenna	Same or smaller	Yes	Yes	No
Triangular SIW antenna	Smaller	Yes	Yes	No
Coupled-fed printed dipole antenna	—	No	No	No
Pyramidal configuration	Larger	No	No	No
Coupled-mode patch	Larger	No	Yes	Yes
Grid array antenna	—	No	Yes	No

hole and aperture. These antennas in [6, 33, 37] require complex fabrication process due to the multilayered structure. The antenna in [38] has difficulty in integration with a planar single-substrate structure due to coaxial feed. Table 1 displays the advantages and disadvantages of the aforementioned wide-beamwidth antenna techniques.

This article proposes a new rectangular microstrip patch antenna using H-shaped gap-coupling with three parasitic radiators to achieve the wide E-plane beamwidth property with horizontal polarization at the K-band of 24–24.25 GHz, which is allocated for the radar application. Side and upper parasitic elements work as radiators resonating at λ and $\lambda/2$, respectively, producing the wide-beamwidth characteristic. The proposed antenna geometry with a planar single substrate contributes to low profile, easy fabrication, and low cost.

2. Antenna Design

The single microstrip patch antenna as the main patch is used for easy integration, being fed by a conducting strip directly connected to the edge of the patch. To widen the E-plane beamwidth, additional patches are required. Two side parasitic patches, of which lengths are twice the length of the main patch, are implemented, and the upper halves of both side patches contribute to the wide E-plane beamwidth. For wider beamwidth, the upper parasitic patch between both side parasitic patches and above the main path is inserted. Consequently, the H-shaped gap-coupled patch antenna is proposed. The geometry of the proposed H-shaped gap-coupled patch antenna, including both side and the upper parasitic patches, was designed on the microwave substrate RO4350B with a thickness of 10 mil and a relative dielectric constant ε_r of 3.48 using commercial Electromagnetic Simulation Software (CST Microwave Studio).

Figure 1 shows the simplified concept of the H-shaped gap-coupled antenna for the wide E-plane beamwidth. The synthesis of the beam patterns of the type A and B antennas gives rise to the wide E-plane beamwidth characteristic of the proposed antenna.

2.1. Main and Both Side Patches (Type A). Each side parasitic square patch with approximate one wavelength is implemented on the same layer of the main square patch. The parasitic elements serve as λ resonated radiators, and the type A antenna includes the main and both side patches, as depicted in Figure 1. The parasitic element of the antenna is primarily magnetically coupled with the feed patch. Figures 2(a) and 2(b) display the radiation patterns and their synthesis produced by four magnetic currents, and Figures 2(c)–2(e) show the E-plane radiation pattern, surface current, and E-field distributions of the type A antenna at 24.1 GHz in simulation, respectively. The lower half of both λ resonated radiators has the same surface current direction as the main patch, and the upper half has the opposite direction. The principle of widening E-plane beamwidth can be explained by the synthesis of the radiation patterns generated by four magnetic currents, $J_{m,m1}$, $J_{m,m2}$, $J_{m,p1}$, and $J_{m,p2}$, in the main and parasitic patches. The magnetic currents $J_{m,m1}$, $J_{m,m2}$, $J_{m,p1}$, and $J_{m,p2}$ are placed with the distance of $0.24\lambda_o$ on y-axis, and the magnitude of $J_{m,p1,2}$ is approximately 0.45 times that of $J_{m,m}$. The magnetic currents $J_{m,p1}$ and $J_{m,p2}$ are placed with the distance of $0.385\lambda_o$ on x-axis. Only considering the peak antenna gain caused by $J_{m,p1}$ and $J_{m,p2}$, the magnitude of the equivalent magnetic current in the middle of both magnetic currents is corresponding to approximately 0.9 times that of $J_{m,m}$ from array factor calculation. The wide-beamwidth property is obtained by the synthesis of the Δ beam pattern generated by $J_{m,m1}$ and $J_{m,p1,2}$ with the

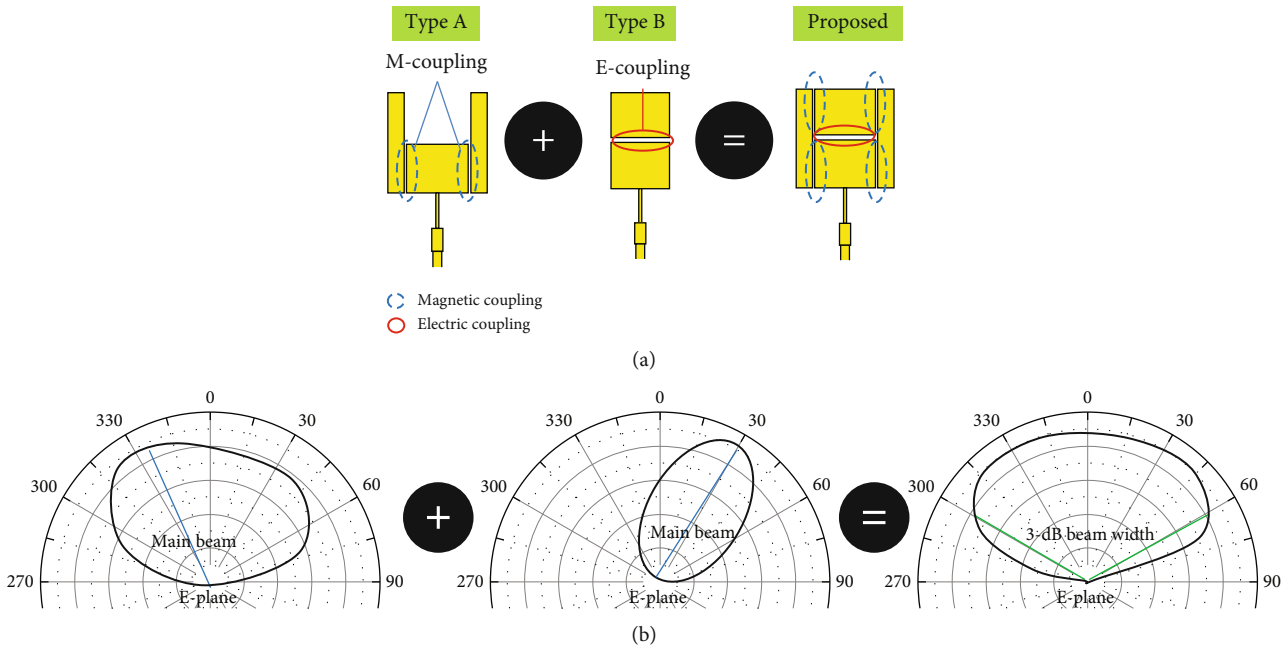

FIGURE 1: Simplified concept of the proposed H-shaped gap-coupled antenna for wide E-plane beamwidth: (a) geometry and (b) beam pattern.

distance of $0.48\lambda_o$ and the additional beam pattern generated by $J_{m,m2}$ being placed at the middle of both $J_{m,m1}$ and $J_{m,p1,2}$. The simulation of type A antenna shows the peak gain of 5.84 dBi and E-plane half-power beamwidth (HPBW) of 112.7° with a main lobe direction of −35° in the elevation plane.

2.2. Main and Upper Patches (Type B). Additional radiation is required in the main lobe direction of the positive angle in the elevation plane to widen the beamwidth. Therefore, an H-shaped gap-coupled patch antenna is introduced that includes the type A antenna and an additional upper parasitic square patch element. The upper parasitic patch with a length of approximately a half wavelength operates as a $\lambda/2$ resonated radiator like the main one. The parasitic element of the antenna is dominantly electrically coupled with the feed patch. Figures 3(a) and 3(b) illustrate the simulated E-plane radiation pattern and surface current of the type B antenna, respectively. The type B antenna has a peak gain of 7.01 dBi, E-plane HPBW of 58.3°, and main lobe direction of 31° in the elevation plane at 24.1 GHz. The type B antenna has the main lobe direction of a positive angle but a high side-lobe level in the elevation plane. The side-lobe of the antenna is caused by surface currents with approximately 180° out of phase, operating at TM_{02} mode in terms of phase. Due to the side-lobe, the H-shaped gap-coupled antenna geometry—comprising the main, upper, and both side patches—has no effect on the enhancement of the E-plane beamwidth. Therefore, the side-lobe of the type B antenna must be removed for the wide-beamwidth characteristic of the entire antenna with H-shaped gap-coupling.

For the phase delay (except for phase reversal) of the upper parasitic patch compared with the fed patch and the wide E-plane beamwidth property of the proposed H-shaped gap-coupled antenna employing type A and B antennas, the proposed H-shaped gap-coupled antenna has been optimized by CST Microwave Studio with the parameters of the length of the upper patch and the gap between the upper and main patches. Consequently, the length of the upper parasitic patch is reduced by 0.1 mm, corresponding to $0.014\lambda_g$, changing the electrical length compared with the driven patch. Figures 3(c)–3(e) illustrate the simulated E-plane radiation pattern and distributions of surface current and E-field of the revised type B antenna. Note that the side-lobe of the previous type B antenna is eliminated. In simulation, it has the peak gain of 7 dBi, E-plane HPBW of 71.9°, and main lobe direction of 19° in the elevation plane at 24.1 GHz.

2.3. Proposed H-Shaped Gap-Coupled Patch Antenna. The design procedure of the proposed H-shaped gap-coupled antenna is as follows: Firstly, a conventional microstrip square patch antenna was designed for the K-band of 24–24.25 GHz. The designed sole main microstrip patch antenna has the peak gain of 6.41 dBi and HPBW of 78.2° and 75.9° in the E- and H-planes, respectively. Secondly, both side parasitic square patches, working as λ resonated radiators, were added to the main patch with coupling gaps between the main and side parasitic patches (type A antenna). The spacings between the fed and side patches were optimized for the wide E-plane beamwidth property, as shown in Figure 4. Finally, the upper parasitic square patch, operating as a $\lambda/2$ resonated radiator, was added to

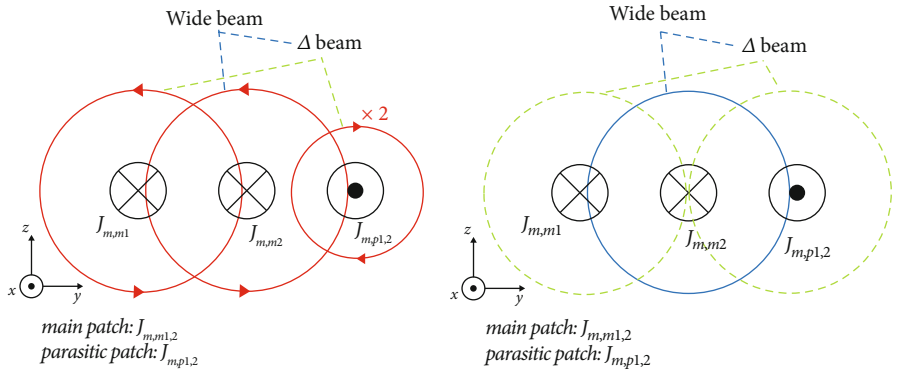

(a) (b)

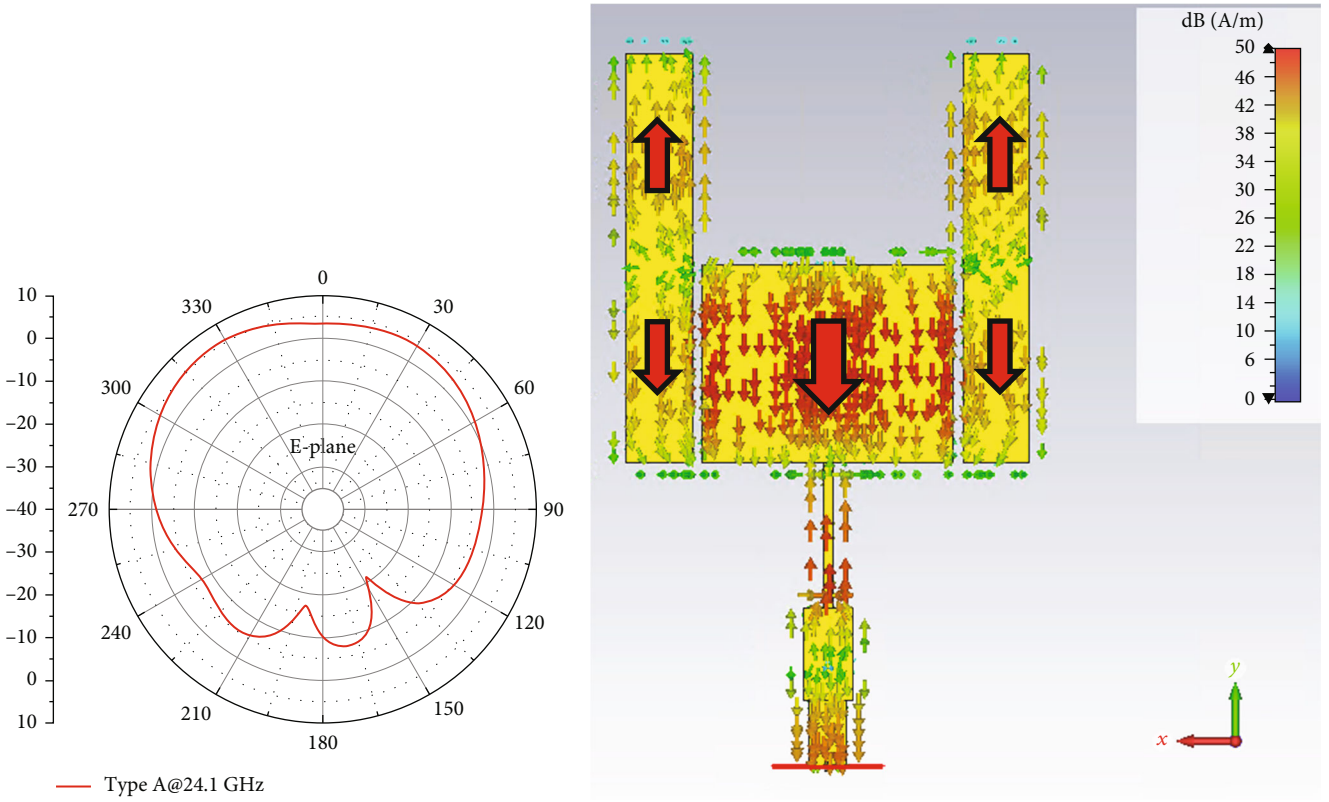

(c) (d)

Figure 2: Continued.

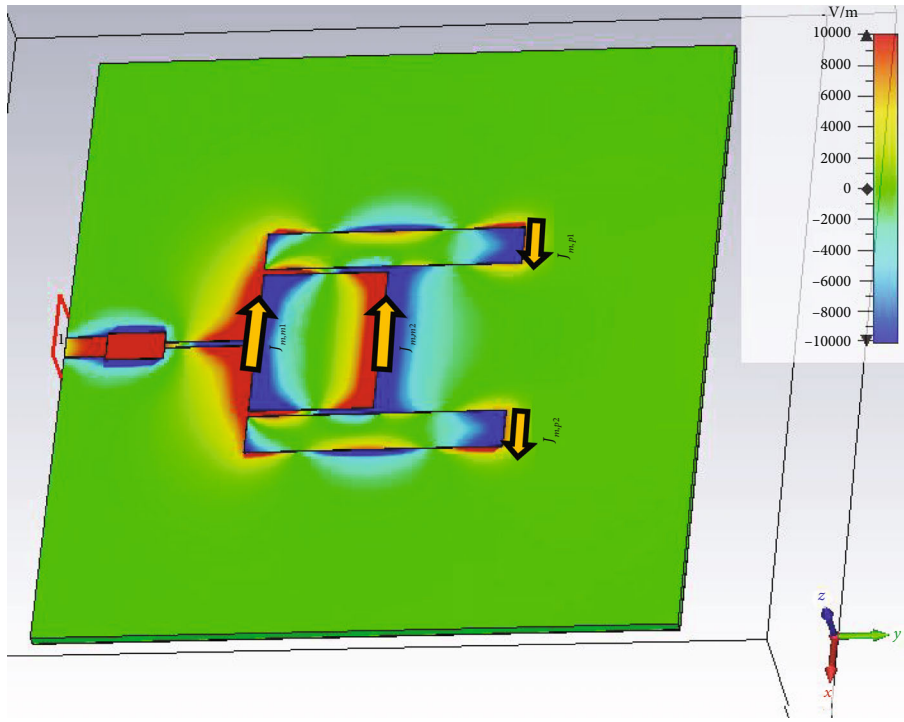

(e)

FIGURE 2: Simulations of the type A antenna at 24.1 GHz: (a) the radiation patterns and (b) their synthesis, (c) E-plane radiation pattern, (d) surface current, and (e) E-field distributions.

the type A antenna with a coupling gap between the main and upper patches and coupling gaps between the upper and side patches (H-shaped gap-coupled antenna). The proposed H-shaped gap-coupled antenna employing the type A and B antennas together has gap-couplings of "driven patch-both side patches," "driven patch-upper patch," and "upper patch-both side patches." The spacings between the fed and upper patches between the fed/upper and side patches were optimized for the wider E-plane beamwidth property compared with the type A antenna, as illustrated in Figure 5. Figure 6 shows the designed H-shaped gap-coupled antenna for the wide E-plane beamwidth characteristic. The dimensions of the H-shaped gap-coupled patch antenna are tabulated in Table 2. Figure 7 illustrates the simulated E-plane radiation pattern and distributions of surface current and E-field of the proposed wide-beamwidth antenna, which are the superimposed results of the type A and revised type B antennas as depicted in Figures 2(d) and 2(e) and 3(d) and 3(e). The proposed H-shaped gap-coupled antenna provides the peak gain of 5.21 dBi and HPBW of 127.4° and 94° in the E- and H-planes at 24.1 GHz in simulation. The lower half of both λ resonated radiators (side patches) has the same surface current direction as the main patch, and the upper half has the opposite direction. Moreover, $\lambda/2$ resonated radiator (upper patch) has phase delay compared with the main patch. The designed planar microstrip antenna can be analyzed using cavity model [1, 39, 40]. As shown in Figures 7(c) and 7(d), considering the E-field intensity, the cavity model of the proposed antenna is depicted with slots S1-S5. When $\varphi = 0$, the radiation pattern in yz-plane can be derived as follows [41]:

$$E_{\theta,\text{total}} = E_{\theta,S1} e^{-j(kl_d \cos\theta)/2} + E_{\theta,S2} + E_{\theta,S3} e^{j\left[\left(kl_g \cos\theta\right)/2+\beta_1\right]} + E_{\theta,S4,5} e^{j[(kl_d \cos\theta)/2+\beta_2]},$$

$$E_{\theta,Sn} = j\frac{hE_{0,Sn}e^{-jk_0 r}}{\pi r} \sin\theta \operatorname{sinc} X_{Sn},$$

$$X_{Sn} = \frac{k_0 W_{Sn} \sin\varphi}{2}, \quad (1)$$

where k is the wave number in free space, l_d is the length of the side patch, l_g is the gap between the main and upper patches, β is the difference in phase excitation compared with the slot 2 ($\beta_2 = \pi$, Figures 2 and 3), θ and φ are the polar and azimuth angles in the coordinated system, E_0 is the maximum amplitude of the electric field, and h and W are the thickness of the substrate and the width of the patch, respectively.

The volume of the proposed H-shaped gap-coupled antenna, including the ground plane, becomes $1.24\lambda_o \times 1.30\lambda_o \times 0.0204\lambda_o$ (λ_o: free-space wavelength). The size reduction can be expected by replacing each patch with a microstrip magnetic dipole antenna consisting of a patch and a metal wall.

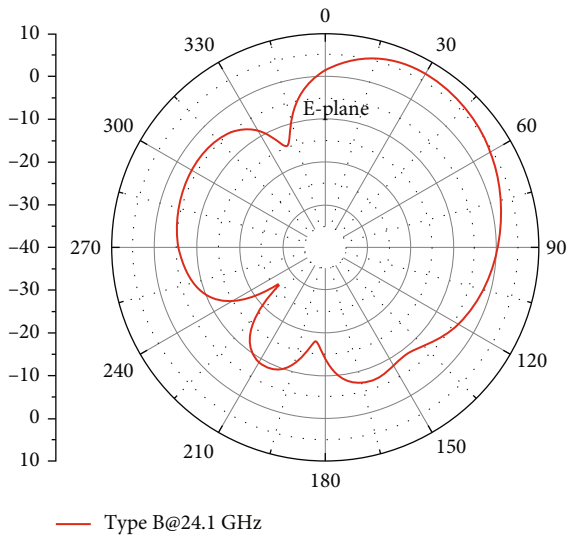

(a)

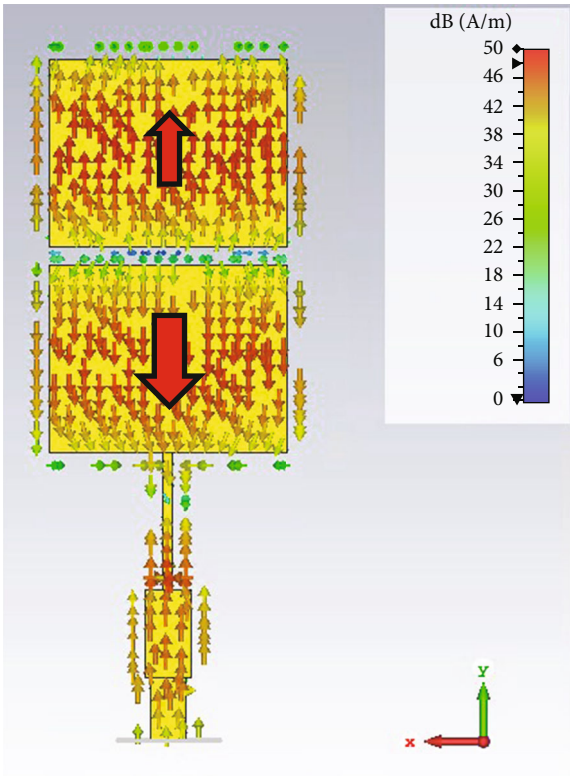

(b)

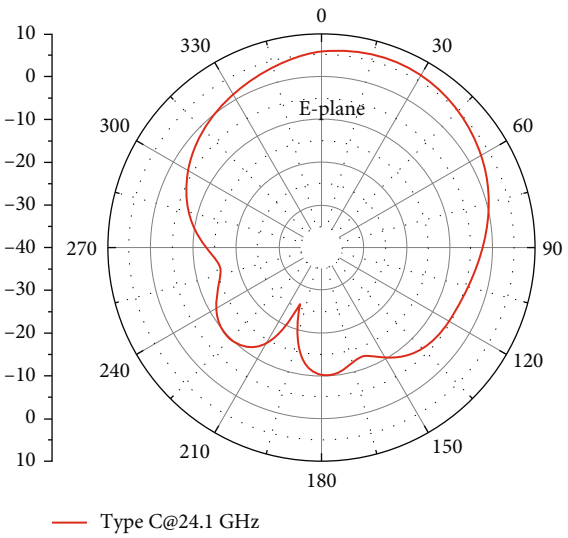

(c)

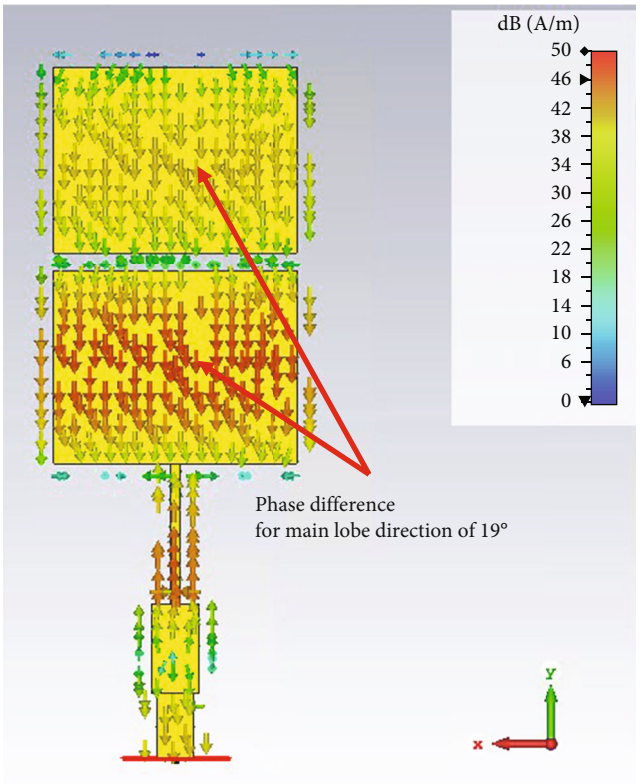

(d)

Figure 3: Continued.

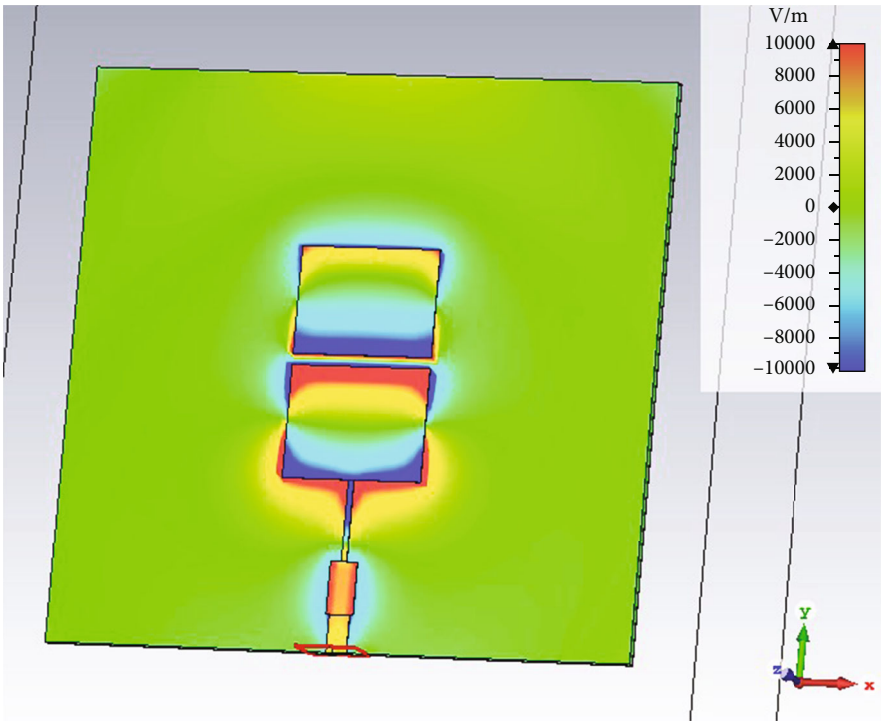

(e)

FIGURE 3: Simulation of the type B antenna at 24.1 GHz before and after revision: (a) E-plane radiation pattern and (b) surface current distribution of the type B antenna with the same patch lengths and (c) E-plane radiation pattern, (d) surface current distribution, and (e) E-field distribution of the revised type B antenna.

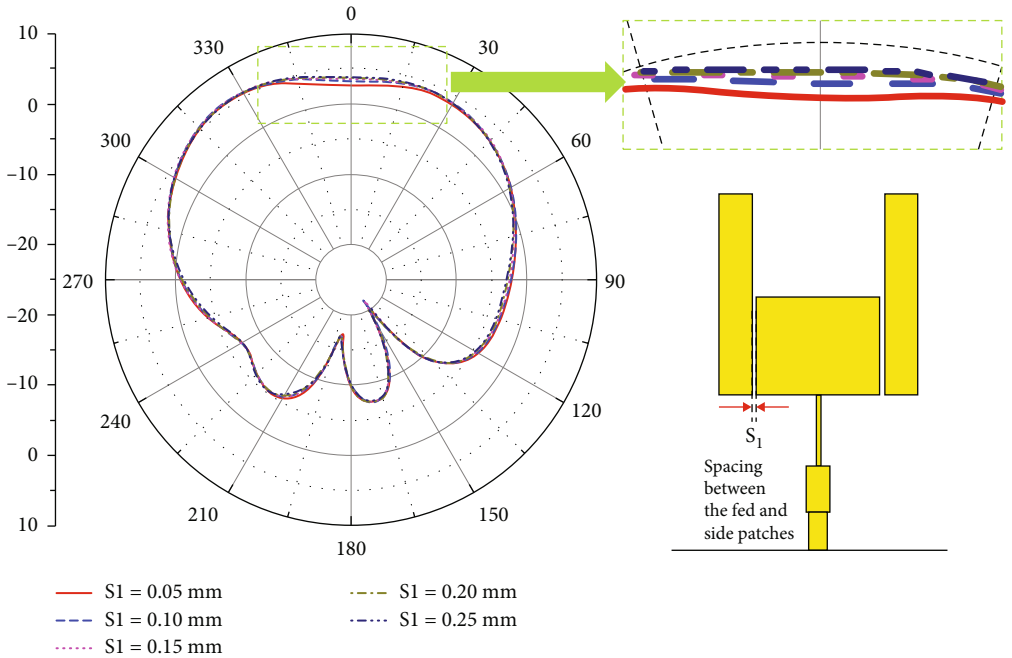

FIGURE 4: Simulated radiation patterns for the type A antenna with different parameter at 24.1 GHz: spacing between the fed and side patches (S_1).

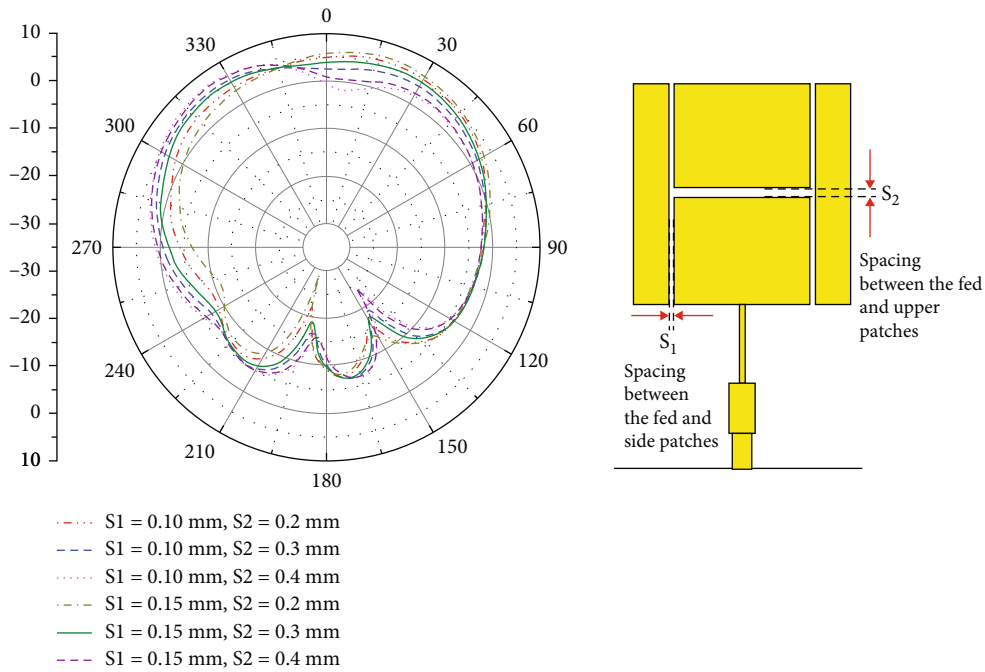

Figure 5: Simulated radiation patterns for the H-shaped gap-coupled antenna with different parameters at 24.1 GHz: spacings between the fed and side patches (S_1) and between the fed and upper patches (S_2).

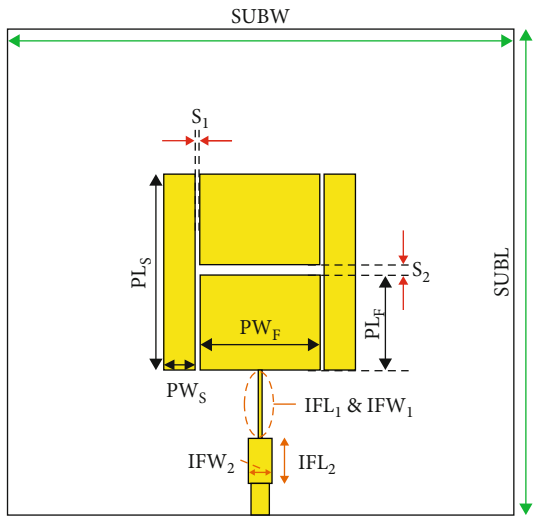

Figure 6: Geometry of the proposed H-shaped gap-coupled patch antenna.

Table 2: Dimensions of the H-shaped gap-coupled patch antenna.

Parameter	Description	Value (mm)
PL_F	Length of the fed patch	2.99
PW_F	Width of the side parasitic patch	3.8
PL_S	Length of the side parasitic patch	6.18
PW_S	Width of the side parasitic patch	1
S_1	Spacing between the fed and side patches	0.15
S_2	Spacing between the fed and upper patches	0.3
ITL_1	Impedance transformer length	2.2
ITW_1	Impedance transformer width	0.15
ITL_2	Impedance transformer length	1.4
ITW_2	Impedance transformer width	0.74
SUBL	Length of the substrate	15.38
SUBW	Width of the substrate	16.1
SUBH	Height of the substrate	0.254

3. Measurement Results

To measure the radiation pattern and return loss, the wide-beamwidth antenna, designed using microstrip line feed with a planar single-substrate structure, is required for an SMA connector. When the tip of the SMA connector is aligned with the signal microstrip line, the body of the SMA connector affects the beam pattern of the antenna due to a relatively short distance from the radiator to the body. To reduce the influence of the body, the proposed wide-beamwidth antenna was designed and fabricated, considering the probe feed to the signal microstrip line, as depicted in Figure 8(a). As a result, the size of the ground plane was enlarged. The radiation pattern of the introduced antenna was measured in anechoic chamber. Figure 9 shows the measurement set-up using compact antenna test range for the radiation pattern.

The simulated and measured return losses, radiation patterns, gains, and efficiencies are illustrated in Figures 8(b)–8(d) and 10, respectively. The center resonant frequency is slightly moved to lower frequency by 0.1 GHz compared

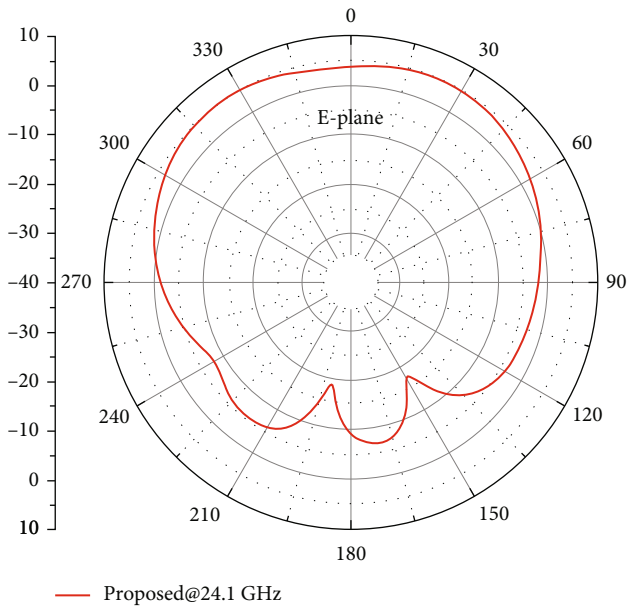

(a)

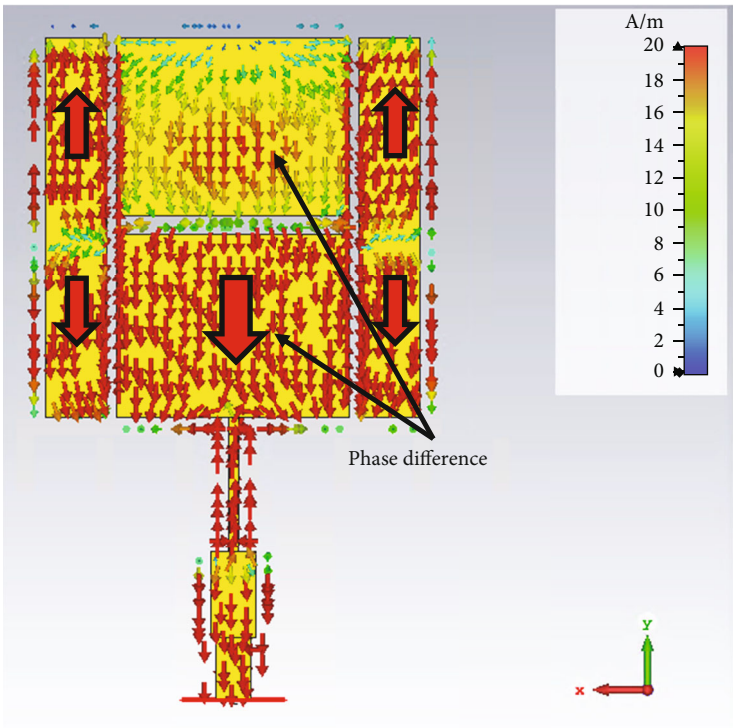

(b)

Figure 7: Continued.

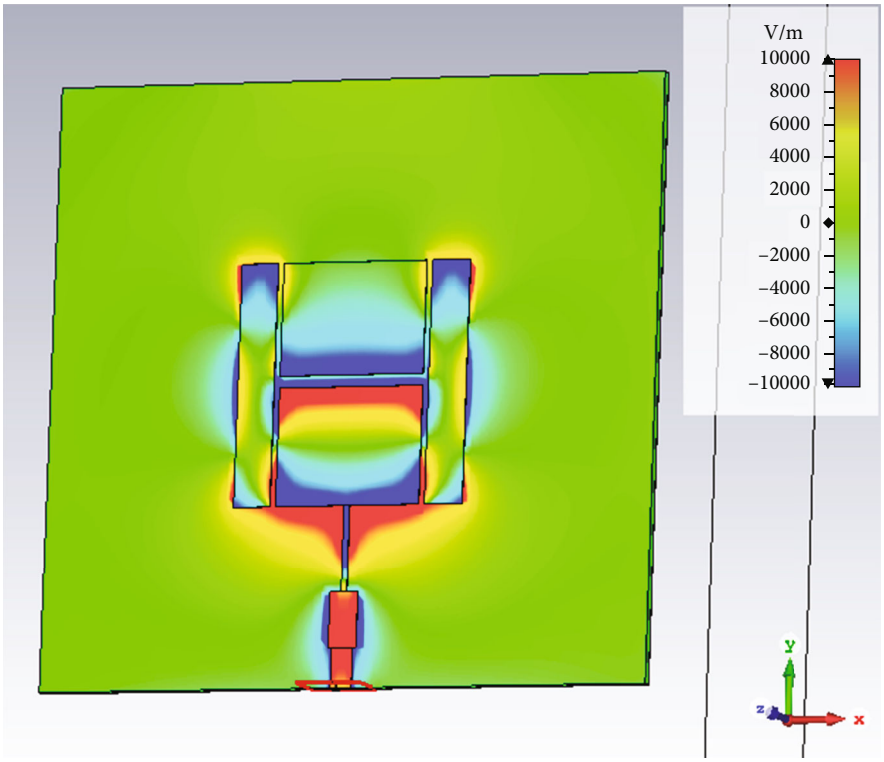

(c)

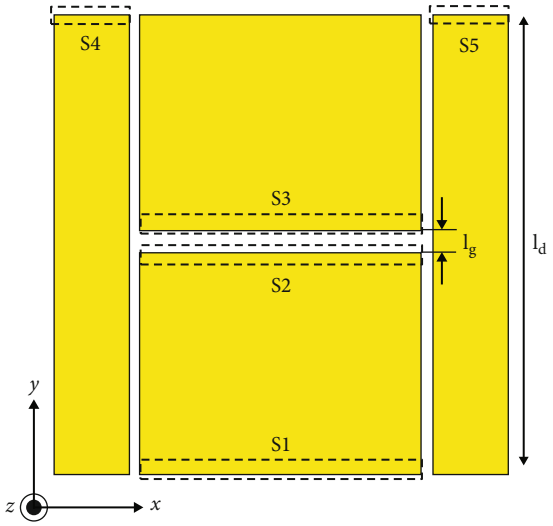

(d)

FIGURE 7: Simulated (a) E-plane radiation pattern, (b) surface current distribution, (c) E-field distribution, and (d) aperture model of the proposed antenna at 24.1 GHz.

with the return loss of the antenna model simulation with the ideal port (Figure 6). The antenna has the impedance bandwidth and fractional bandwidth (FBW) of 510 MHz (23.765–24.275 GHz) and 2.1% for a return loss of greater than 10 dB, respectively.

The simulated gains and E-plane HPBWs are 5.56 dBi and 137.9°, respectively, at the center frequency of 24.1 GHz. The measured gain and E-plane HPBW were 4.82 dBi and 143.4°, respectively, at a center frequency of 24.1 GHz. The maximum detection range for a radar system can be determined as follows [42]:

$$R_{\max} = \left[\frac{P_T G_T G_R \lambda^2 \sigma}{(4\pi)^3 S_{\min}}\right]^{1/4}, \quad (2)$$

where P_T, G_T, G_R, λ, σ, and $S_{\min}$ are the transmit power, transmit antenna gain, receive antenna gain, operating

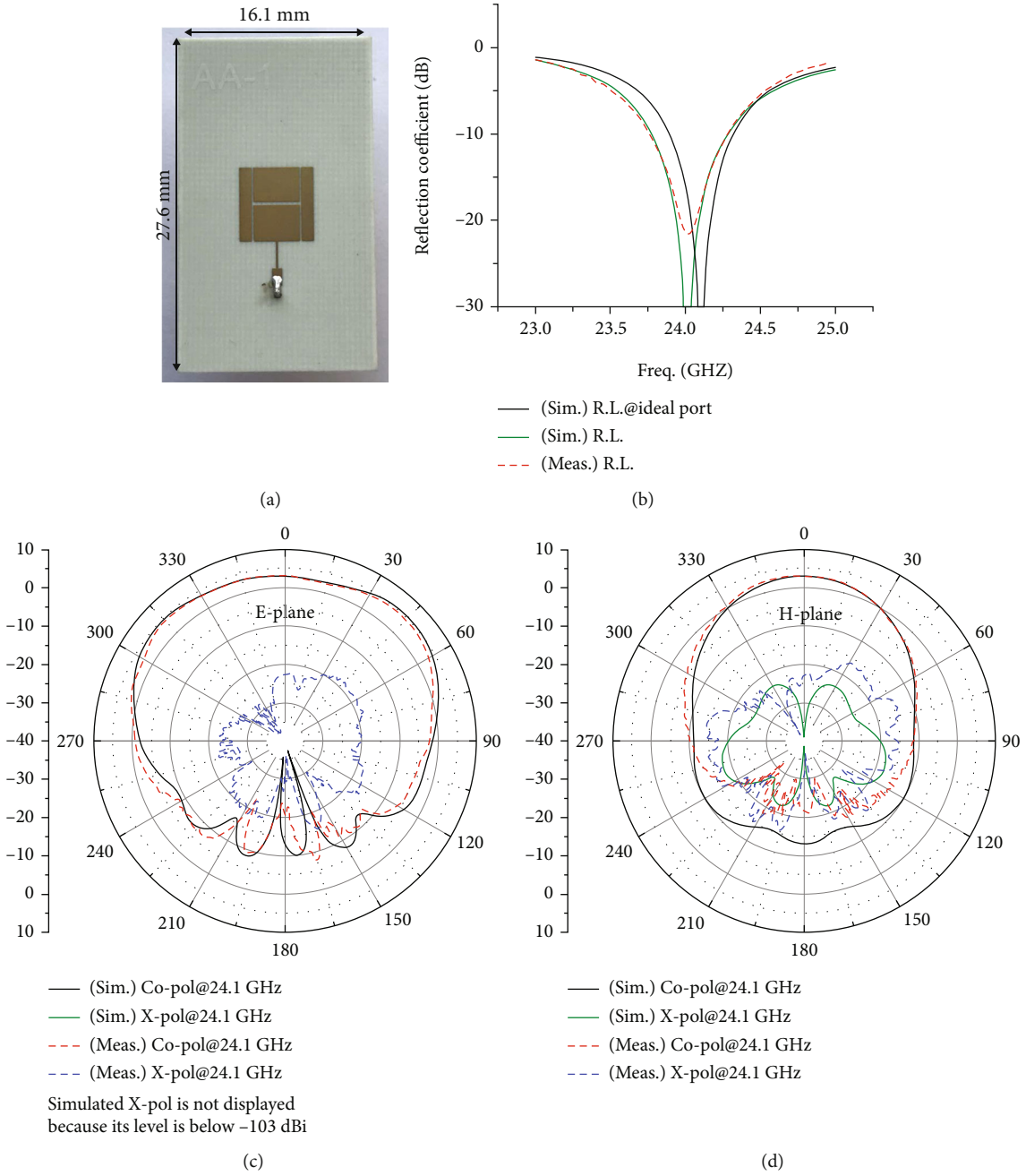

FIGURE 8: Simulated and measured results of the designed wide-beamwidth gap-coupled patch antenna: (a) fabricated picture, (b) return losses, and (c) E- and (d) H-plane radiation patterns.

wavelength, radar cross-section value, and receiver sensitivity, respectively. When a radar system requires higher antenna gain, an array adopting the proposed antenna can be used, while maintaining the wide E-plane beamwidth property.

The simulated and measured antenna efficiencies were 79.1% and 75.3%, respectively, at a center frequency of 24.1 GHz. The measured results agree reasonably well with the simulated results. The discrepancies in simulated and measured results for gains and HPBWs would be mainly attributed to manufacturing tolerances and dielectric loss at the K-band. The fabricated antenna, which uses the SMA connector, has a wider E-plane HPBW compared with the proposed antenna described in Section 2.3 with the ideal port, due to the larger size of its ground plane.

The ratio of the maximum copolarization to cross-polarization radiation levels (the co-to-cross-pol ratio) is used to evaluate the polarization purity. Within the beamwidth of interest, the co-to-cross-pol ratio can be calculated from [43]

$$\text{Co} - \text{to} - \text{cross} - \text{pol ratio} = \frac{\text{maximum copolarization radiation level}}{\text{maximum cross} - \text{polarization radiation level}}. \quad (3)$$

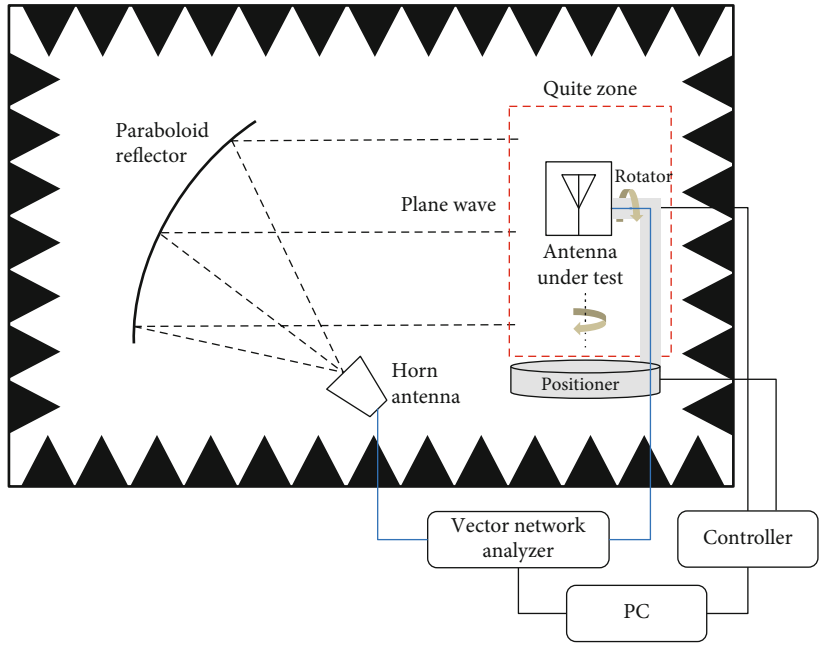

FIGURE 9: Measurement set-up using compact antenna test range.

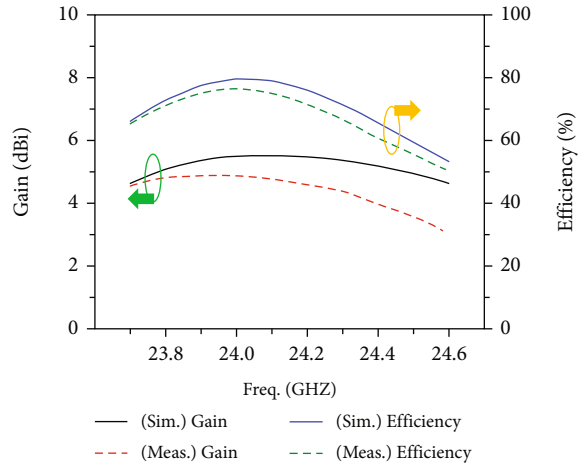

FIGURE 10: Simulated and measured gains and efficiencies of the designed wide-beamwidth gap-coupled patch antenna.

The measured co-to-cross-pol ratios in the E- and H-planes were 19.8 and 17.3 dB over the entire angular range and 22.7 and 20.2 dB within the HPBW, respectively. The measured co-to-cross-pol ratios are acceptable, considering the cross-polarization of the conventional microstrip antenna of approximately 20 dB in the H-plane due to the effect of transverse current [44].

Table 3 shows a performance comparison of the previous reported K-band wide-beamwidth antennas in terms of the total volume, including ground plane size, HPBW, FBW, gain, front-to-back ratio (FTBR), and figures-of-merit (FOMs). Several FOMs are defined by HPBW and gain, related to the antenna's total volume with the ground plane size [25]. FOM_1, FOM_2, and FOM_3 are defined as

$$\begin{aligned} FOM_1 &= \frac{HPBW(\text{degree})^*}{\text{total volume with ground plane}\left(\lambda_O{}^3\right)}, \\ FOM_2 &= \frac{\text{Gain(abs)}}{\text{total volume with ground plane}\left(\lambda_O{}^3\right)}, \\ FOM_3 &= \frac{\text{Gain(abs)} \times HPBW(\text{degree})^*}{\text{total volume with ground plane}\left(\lambda_O{}^3\right)}, \end{aligned} \tag{4}$$

where HPBW* is the wider HPBW for the E- or H-plane.

The proposed H-shaped gap-coupled antenna provided superior FOM performances to other antennas for the K-band. Furthermore, the designed antenna contributes to

Table 3: Performance comparison of the published wide-beamwidth antennas for the K-band.

Ref.	Freq. (GHz)	Total volume with ground plane	HPBW[1]	FBW[2]	Gain (dB)	FOM_1 (BPBW/λ_o^3)	FOM_2 (gain/λ_o^3)	FOM_3 (gain•BPBW/λ_o^3)	Multilayers	Note
[6]	23.8	$2.89\lambda_o \times 5.29\lambda_o \times 0.129\lambda_o$	130°	14.5%	12.2	66	8.4	1,092	O	Conducting via parasitic loop, 1 × 8 arrays
	23.7	$2.92\lambda_o \times 5.68\lambda_o \times 0.129\lambda_o$	150°	16.9%	11.1	70	6.0	904	O	Conducting via parasitic mushroom-like elements, 1 × 8 arrays
[33]	24.25	$3.13\lambda_o \times 1.00\lambda_o \times 0.057\lambda_o$	140°	5.4%	8	776	35.0	4,896	O	Magnetic dipole, 1 × 4 arrays
[37]	24	$4.8\lambda_o \times 2.4\lambda_o \times 0.04\lambda_o$	140°	5.8%	10.5	304	24.3	3,409	O	Coupled-mode patch, 1 × 8 arrays
[38]	24	$1.44\lambda_o \times 11.68\lambda_o \times 0.128\lambda_o$	145°	25%	11.59	67	6.7	971	X	Grid array, two rows with 16 and 17 elements
This work	24.1	$1.30\lambda_o \times 2.22\lambda_o \times 0.0204\lambda_o$	143.4°	2.1%	4.82	2,451	51.8	7,435	X	Parasitic elements with H-shaped gap-coupling

[1]Wider half-power beamwidth for E- or H-plane. [2]Fractional bandwidth.

keeping a planar single substrate, which results in easy fabrication and low cost compared with other antenna structures requiring multilayer fabrication process.

4. Conclusion

This article proposed and fabricated a new wide E-plane beamwidth patch antenna that introduces H-shaped gap-coupling with three parasitic elements for the K-band of 24–24.25 GHz. The side and upper parasitic elements operate as λ and $\lambda/2$ resonators gap-coupled by the driven rectangular patch. The wide E-plane beamwidth property was achieved by synthesizing the radiation patterns of the total radiators. The proposed antenna with a planar single-substrate structure contributes to low profile, easy fabrication, and low cost. The measured co-to-cross-pol ratios for the E- and H-planes are reasonable. The designed antenna illustrates excellent FOMs compared with the other wide-beamwidth antennas for the K-band. Furthermore, the size reduction can be anticipated by replacing each patch with a microstrip magnetic dipole antenna including a patch and a metal wall.

Data Availability

Data are available upon request.

Conflicts of Interest

The authors declare that they have no conflicts of interest.

Acknowledgments

This research was supported by the Basic Science Research Program through the National Research Foundation of Korea (NRF) funded by the Ministry of Education (NRF-2018R1D1A1B07050620).

References

[1] Z. N. Chen, W. K. Toh, and X. Qing, "A microstrip patch antenna with broadened beamwidth," *Microwave and Optical Technology Letters*, vol. 50, no. 7, pp. 1885–1888, 2008.

[2] W.-H. Zhang, Q. Xue, S. Liao, W. Che, and W. Yang, "Low-profile compact microstrip magnetic dipole antenna with large beamwidth and broad bandwidth for vehicular applications," *IEEE Transactions on Vehicular Technology*, vol. 70, no. 6, pp. 5445–5456, 2021.

[3] N. Agrawal, A. K. Gautamak, and R. Mishra, "Design of low volume circularly polarized annular ring-shaped planar antenna for GPS applications," *International Journal of RF and Microwave Computer-Aided Engineering*, vol. 31, no. 7, article e22698, 2021.

[4] T. Mondal, S. Maity, R. Ghatak, and S. R. B. Chaudhuri, "Compact circularly polarized wide-beamwidth fern-fractal-shaped microstrip antenna for vehicular communication," *IEEE Transactions on Vehicular Technology*, vol. 67, no. 6, pp. 5126–5134, 2018.

[5] J.-H. Park, J.-E. Roh, and M.-Q. Lee, "Decoupling network for closely spaced Tx/Rx antennas using a directional coupler and transmission lines," *International Journal of Antennas and Propagation*, vol. 2023, Article ID 5557062, 15 pages, 2023.

[6] C.-A. Yu, E. S. Li, H. Jin et al., "24 GHz horizontally polarized automotive antenna arrays with wide fan beam and high gain," *IEEE Transactions on Antennas and Propagation*, vol. 67, no. 2, pp. 892–904, 2019.

[7] S. Ko and J. Lee, "Hybrid zeroth-order resonance patch antenna with broad E-plane beamwidth," *IEEE Transactions on Antennas and Propagation*, vol. 61, no. 1, pp. 19–25, 2013.

[8] Z. Pan, W. Lin, and Q. Chu, "Compact wide-beam circularly-polarized microstrip antenna with a parasitic ring for CNSS application," *IEEE Transactions on Antennas and Propagation*, vol. 62, no. 5, pp. 2847–2850, 2014.

[9] X. Chen, P. Qin, Y. J. Guo, and G. Fu, "Low-profile and wide-beamwidth dual-polarized distributed microstrip antenna," *IEEE Access*, vol. 5, pp. 2272–2280, 2017.

[10] J. Kornprobst, K. Wang, G. Hamberger, and T. F. Eibert, "A mm-wave patch antenna with broad bandwidth and a wide angular range," *IEEE Transactions on Antennas and Propagation*, vol. 65, no. 8, pp. 4293–4298, 2017.

[11] S. Chattopadhyay, J. Y. Siddiqui, and D. Guha, "Rectangular microstrip patch on a composite dielectric substrate for high-gain wide-beam radiation patterns," *IEEE Transactions on Antennas and Propagation*, vol. 57, no. 10, pp. 3325–3328, 2009.

[12] K. Ng, C. H. Chan, and K. Luk, "Low-cost vertical patch antenna with wide axial-ratio beamwidth for handheld satellite communications terminals," *IEEE Transactions on Antennas and Propagation*, vol. 63, no. 4, pp. 1417–1424, 2015.

[13] H. He, "A novel wide beam circular polarization antenna - microstrip-dielectric antenna," in *2002 3rd International Conference on Microwave and Millimeter Wave Technology*, pp. 381–384, Beijing, China, 2002.

[14] C.-L. Tang, J.-Y. Chiou, and K.-L. Wong, "Beamwidth enhancement of a circularly polarized microstrip antenna mounted on a three-dimensional ground structure," *Microwave and Optical Technology Letters*, vol. 32, no. 2, pp. 149–153, 2022.

[15] T. P. Wong and K. M. Luk, "A wide bandwidth and wide beamwidth CDMA/GSM base station antenna array with low backlobe radiation," *IEEE Transactions on Vehicular Technology*, vol. 54, no. 3, pp. 903–909, 2005.

[16] C.-W. Su, S.-K. Huang, and C.-H. Lee, "CP microstrip antenna with wide beamwidth for GPS band application," *Electronics Letters*, vol. 43, no. 20, pp. 1062-1063, 2007.

[17] L. Chen, T.-L. Zhang, C. Wang, and X.-W. Shi, "Wideband circularly polarized microstrip antenna with wide beamwidth," *IEEE Antennas and Wireless Propagation Letters*, vol. 13, pp. 1577–1580, 2014.

[18] X. L. Bao and M. J. Ammann, "Dual-frequency dual circularly-polarised patch antenna with wide beamwidth," *Electronics Letters*, vol. 44, no. 21, pp. 1233-1234, 2008.

[19] T. Tan, Y. Xia, and Q. Zhu, "A novel wide beamwidth and circularly polarized microstrip antenna loading annular dielectric superstrate with metal ring," in *2014 IEEE Antennas and Propagation Society International Symposium (APSURSI)*, pp. 1883-1884, Memphis, TN, USA, 2014.

[20] M. Tang, Z. Wu, T. Shi, and R. W. Ziolkowski, "Dual-band, linearly polarized, electrically small Huygens dipole antennas," *IEEE Transactions on Antennas and Propagation*, vol. 67, no. 1, pp. 37–47, 2019.

[21] M.-C. Tang, Z. Wu, T. Shi, H. Zeng, W. Lin, and R. W. Ziolkowski, "Dual-linearly polarized, electrically small, low-profile,

broadside radiating, Huygens dipole antenna," *IEEE Transactions on Antennas and Propagation*, vol. 66, no. 8, pp. 3877–3885, 2018.

[22] M. Tang, H. Wang, and R. W. Ziolkowski, "Design and testing of simple, electrically small, low-profile, Huygens source antennas with broadside radiation performance," *IEEE Transactions on Antennas and Propagation*, vol. 64, no. 11, pp. 4607–4617, 2016.

[23] G. Yang, J. Li, J. Yang, and S.-G. Zhou, "A wide beamwidth and wideband magnetoelectric dipole antenna," *IEEE Transactions on Antennas and Propagation*, vol. 66, no. 12, pp. 6724–6733, 2018.

[24] L. Ge and K. M. Luk, "A low-profile magneto-electric dipole antenna," *IEEE Transactions on Antennas and Propagation*, vol. 60, no. 4, pp. 1684–1689, 2012.

[25] L. Ge and K. M. Luk, "A magneto-electric dipole antenna with low-profile and simple structure," *IEEE Antennas and Wireless Propagation Letters*, vol. 12, pp. 140–142, 2013.

[26] C. Ding and K.-M. Luk, "Low-profile magneto-electric dipole antenna," *IEEE Antennas and Wireless Propagation Letters*, vol. 15, pp. 1642–1644, 2016.

[27] Y. Kim, H. Dong, K. Kim, and H. L. Lee, "Compact planar multipole antenna for scalable wide beamwidth and bandwidth characteristics," *IEEE Transactions on Antennas and Propagation*, vol. 68, no. 5, pp. 3433–3442, 2020.

[28] C. Liu, S. Xiao, H. Tu, and Z. Ding, "Wide-angle scanning low profile phased array antenna based on a novel magnetic dipole," *IEEE Transactions on Antennas and Propagation*, vol. 65, no. 3, pp. 1151–1162, 2017.

[29] C.-M. Liu, S. Xiao, and X.-L. Zhang, "A compact, low-profile wire antenna applied to wide-angle scanning phased array," *IEEE Antennas and Wireless Propagation Letters*, vol. 17, no. 3, pp. 389–392, 2018.

[30] J. Yoo, S. Khang, T. Yeo, and J. Yu, "Compact meander magnetic dipole antenna for wide-angle scanning," in *2018 IEEE International Symposium on Antennas and Propagation & USNC/URSI National Radio Science Meeting*, pp. 1611-1612, Boston, MA, USA, 2018.

[31] J. Liu and Q. Xue, "Microstrip magnetic dipole Yagi array antenna with endfire radiation and vertical polarization," *IEEE Transactions on Antennas and Propagation*, vol. 61, no. 3, pp. 1140–1147, 2013.

[32] A. Boukarkar, X. Q. Lin, and Y. Jiang, "A dual-band frequency-tunable magnetic dipole antenna for WiMAX/WLAN applications," *IEEE Antennas and Wireless Propagation Letters*, vol. 15, pp. 492–495, 2016.

[33] Z. Yi, R. Zhange, B. Xu et al., "A wide-angle beam scanning antenna in E-plane for K-band radar sensor," *IEEE Access*, vol. 7, pp. 171684–171690, 2019.

[34] H. Y. Cho, B. K. Ahn, H.-W. Jo, J.-W. Kim, S. Kim, and J.-W. Yu, "Quasi-hemispherical region scanning phased array system using triangular SIW antenna elements with short ends," *IEICE Electron Express*, vol. 17, no. 8, pp. 1–3, 2020.

[35] S. S. Wang, S. J. Yoo, J. S. Park, H. S. Shim, and H. S. Choo, "Design of a broadband coupled-fed printed dipole antenna as an array element for direction finding systems," *Journal of Electromagnetic Engineering and Science*, vol. 19, no. 4, pp. 266–271, 2019.

[36] R. Mittra, R. Yang, M. Itoh, and M. Arakawa, "Microstrip patch antennas for GPS applications," in *Proceedings of IEEE Antennas and Propagation Society International Symposium*, pp. 1478–1481, Ann Arbor, MI, USA, 1993.

[37] X. Yang and X. Liu, "Design of a wide-beam microstrip array antenna for automotive radar application," *IEEE Access*, vol. 9, pp. 142340–142347, 2021.

[38] M. G. N. Alsath, L. Lawrance, and M. Kanagasabai, "Bandwidth-enhanced grid array antenna for UWB automotive radar sensors," *IEEE Transactions on Antennas and Propagation*, vol. 63, no. 11, pp. 5215–5219, 2015.

[39] A. G. Derneryd, "Linearly polarized microstrip antennas," *IEEE Transactions on Antennas and Propagation*, vol. 24, no. 6, pp. 846–851, 1976.

[40] W. F. Richards, Y. T. Lo, and D. D. Harrison, "An improved theory for microstrip antennas and applications," *IEEE Transactions on Antennas and Propagation*, vol. 29, no. 1, pp. 38–46, 1981.

[41] C. A. Balanis, *Antenna Theory: Analysis and Design*, Wiley, New York, 3rd ed. edition, 2005.

[42] Y. Chen, J. Li, F. Ding, and L. Cao, "Antenna in package design and measurement for millimeter-wave applications in fan-out wafer-level package," *IEICE Electron Express*, vol. 19, no. 14, p. 20220122, 2022.

[43] Z. N. Chen and M. Y. W. Chia, *Broadband Planar Antennas: Design and Applications*, John Wiley & Sons, Hoboken, NJ, 2005.

[44] J. Ma, S.-L. Tan, S.-Y. Ni et al., "Cross-polarization suppression by comb-shaped slots in microstrip patch," in *2021 International Conference on Microwave and Millimeter Wave Technology (ICMMT)*, pp. 1–3, Nanjing, China, 2021.